Applied Physics Letters

Using methodical compositional tuning to optimize Co_xTb_{1-x} structural and magnetic properties

Cite as: Appl. Phys. Lett. **118**, 212405 (2021); https://doi.org/10.1063/5.0049224
Submitted: 02 March 2021 • Accepted: 03 May 2021 • Published Online: 25 May 2021

Brandon Wilfong, W. L. N. C. Liyanage, Jared Naphy, et al.

Applied Physics Letters ARTICLE scitation.org/journal/apl

Using methodical compositional tuning to optimize Co_xTb_{1-x} structural and magnetic properties

Cite as: Appl. Phys. Lett. **118**, 212405 (2021); doi: 10.1063/5.0049224
Submitted: 2 March 2021 · Accepted: 3 May 2021 ·
Published Online: 25 May 2021

Brandon Wilfong,[1] W. L. N. C. Liyanage,[2] Jared Naphy,[1] Dustin A. Gilbert,[2,3] Steven P. Bennett,[4] and Michelle E. Jamer[1,a)]

AFFILIATIONS

[1]Physics Department, United States Naval Academy, Annapolis, Maryland 20899, USA
[2]Department of Physics and Astronomy, University of Tennessee, Knoxville, Tennessee 37996, USA
[3]Materials Science and Engineering, University of Tennessee, Knoxville, Tennessee 37996, USA
[4]Material Science and Technology Division, U.S. Naval Research Laboratory, Washington, DC 20375, USA

[a)]Author to whom correspondence should be addressed: jamer@usna.edu

ABSTRACT

The Co-rich end of the Co–Tb binary phase diagram (Co_xTb_{1-x}, x = 0.66–0.82) has been investigated to understand the phases which form in the bulk and how they interact to yield magnetic behavior which has been reported to be ideal for use in spintronic devices. This work shows that the phases and phase fractions present across this composition range follow those predicted by the binary phase diagram, and all compounds in this composition range are multiphase. Magnetic measurements show similar behavior in this composition range to related thin film work, and we attribute the observed behavior to the respective binary phases present in each compound. Ideal magnetic behavior of minimized magnetic saturation and maximized coercivity is observed in the range of $x = 0.78 - 0.80$ related to the majority phase Co_7Tb_2 in these two compounds. High pressure magnetic measurements show magnetic saturation and coercivity at 300 K change little with respect to external pressure. The extension of the synthesis of these binaries into the bulk allows for specific binary phases to be targeted and analyzed for consideration in future devices.

Published by AIP Publishing. https://doi.org/10.1063/5.0049224

Since Berger and Slonczewski independently predicted that electrical currents can be effectively used to change the magnetization of a material,[1,2] there has been an explosion of work focusing on implementing these phenomena. These systems incorporate magnetization control by electrical currents and have spawned the heavily researched field of spintronics.[3–5] The main advantages in using spin currents, compared to other alternatives such as current-generated magnetic fields, are the higher energy efficiency and scalability of these devices.[6] Traditionally, spintronic devices which leverage direct control via charge currents were ferromagnetic and arranged into device stacks. This was done in order to realize spin valves and magnetic tunnel junctions utilizing the spin transfer torque (STT) effect.[7–10] The STT approach requires high current densities and increases in efficiency, motivating an alternative mechanism of control through the use of spin-polarized charge currents, called spin–orbit torque (SOT).[11–13]

Although ferromagnetic materials have dominated this field of spintronics, antiferromagnetic materials have recently been studied for use in these devices.[5,14] Antiferromagentic materials have the benefit of zero internal magnetic moment, which limits potential magnetic field interference within the device. This has noted benefits, such as decreased stray magnetic field sensitivity allowing higher density on devices as well as faster dynamics due to the higher switching frequencies possible using antiferromagenetic materials. As such, recent work has developed spin valve and magnetic tunnel junction analogues using antiferromagentic materials in order to understand how the STT and SOT effects can be utilized with these materials.[15–19] From a fundamental point of view, material exploration is currently required to find antiferromagnetic and/or ferrimagentic materials with ideal properties at room temperature to allow for optimized device manufacturing.

Rare-earth-containing transition metal alloys are promising candidates for application in antiferromagentic/ferrimagnetic spintronic devices.[14,20] In these materials, the magnetic exchange between the 3*d* electrons of the transition metal and 4*f* electrons of the rare-earth

metal stabilizes room temperature ferrimagentic order depending on the concentration of each constituent in the alloy.[21] The majority of work done has been focused on thin films of rare-earth transition metal alloys[21–25] and have successfully shown that spin–orbit torque switching can be achieved in this class of materials. In particular, Co–Tb alloys (Co_xTb_{1-x}) have been studied extensively and shown to have ideal properties at room temperature in the cobalt-rich range ($x > 0.70$) of the phase diagram.[23,26–29] This range has been shown to contain the magnetic compensation point in this phase space where the magnetic moment saturation goes to zero, coercivity diverges, and spin–orbit torque efficiency reaches a maximum.[23,27,28]

This work is complementary to the aforementioned work on thin film integrated devices which show Co_xTb_{1-x} alloys as suitable materials for ferrimagentic spin–orbit torque device materials. The thin films are crystallographically amorphous as-synthesized[21,23] and thus a fundamental understanding of the phases present and how they interact is lacking. In this work, we have synthesized the range of cobalt-rich Co_xTb_{1-x} alloys in bulk through arc-melting and the samples synthesized herein are not amorphous which affords us the ability to undertake extensive crystallographic analysis. This allows us to better understand the phases present at the macroscale through synchrotron x-ray diffraction (XRD) and elemental analysis. The samples synthesized herein are not amorphous which affords us the ability to undertake extensive crystallographic analysis. We have then studied the magnetic properties of these bulk samples under ambient conditions and moderate pressure to track how composition changes affect the magnetic properties. It should be noted that there may not be a clear direct correspondence between bulk samples and thin films samples with regard to composition and phases due to the non-equilibrium growth conditions which can be present in thin film growth procedures. However, this work highlights which phases are likely present in the corresponding thin films and shows that the bulk samples show similar behavior with regard to composition and magnetic properties to the thin film analogues.

Bulk samples of Co_xTb_{1-x} (x = 0.66–0.82) were synthesized via arc-melting of elements in corresponding stoichiometric ratios using an Edmund Buehler MAM-1 under ultra-high purity Ar atmosphere. The arc-melted ingots were loaded into quartz tubes and sealed under moderate vacuum ($<10^{-2}$ Torr). The samples were then annealed at 1050 °C for 48 h before quenching in an ice bath. High-resolution synchrotron x-ray diffraction was performed on powders of ground as-recovered ingots at Beamline 11-BM at the Advanced Photon Source at Argonne National Lab. Ground powders were packed in 0.4 mm Kapton capillary tubes and sealed with clay under atmospheric conditions. Diffraction data were collected between 0.5° and 46° with a step size of 0.0001° using a constant wavelength of 0.457 921 Å at 300 K. Rietveld refinements and data analysis was performed using the GSAS software suite.[30] The high pressure magnetic properties of pieces of the as-synthesized bulk samples were measured under uniaxial pressures of 0 MPa, 5.5 MPa, 11 MPa, and 16.5 MPa, applied by a BeCu pressure cell. Magnetization vs temperature measurements were performed by applying a static field of 10 mT and cooling from 400 K to 2 K. Magnetic hysteresis loops (M-H) were measured between ±5 T at 2 K, 50 K, 200 K, and 300 K. Energy dispersive x-ray spectroscopy spectra were collected on a LEO SEM/energy-dispersive x-ray analysis system at a beam energy of 20 kV. The tabulated compositions were obtained as an averages of five different sites collected from a cleaved edge surface of each specimen.

The majority of work on Co–Tb binary alloys have focused on thin film synthesis methods for ease of coupling these systems within devices. However, one downside to this method is that as-synthesized Co–Tb thin films are amorphous and their crystallographic and compositional nature are difficult to ascertain.[23,28] Thus, our work investigates this phase diagram in the bulk to understand what binary phases are present across this phase space and how they interact to yield the desired magnetic properties reported in previous work.[23,27,28] In order to determine the phases present in each sample, arc-melted and annealed ingots were crushed and ground into powders for high-resolution synchrotron powder x-ray diffraction (XRD) performed at 11-BM at Argonne National Lab. These data were subsequently analyzed through Rietveld refinement in order to extract lattice parameters and phase fraction of each Co–Tb and Tb–O binary present in the sample. A representative powder XRD pattern and corresponding Rietveld refinement fit are presented in Fig. 1; remaining powder XRD patterns and Rietveld refinements are presented in supplementary material.

A summary of all sample across the phase space investigated for $Co_{1-x}Tb_x$ ($x = 0.66 - 0.82$) is presented in Table I and Fig. 2 which shows the phase fractions of each binary present in the sample as well as elemental analysis from EDS and calculated from Rietveld refinement. In general, the phase fractions of each binary correspond well with the established Co–Tb phase diagram.[31] There are no unknown phases present that are not well documented in the Co–Tb or Tb–O phase space in any of the other powder XRD patterns presented in the Supplemental Information. Although these ingots were annealed after arc-melting, we do see multiple phases present in each sample even for compositions which should be within single phase stoichiometry regions of the phase diagram. As such, an additional study to optimize post-synthesis annealing or using other synthesis methods could be employed if single phase samples within this Co-rich end of the phase diagram are desired.

Elemental analysis from EDS, as well as calculated composition from phase fractions and stoichiometry of binary phases in each

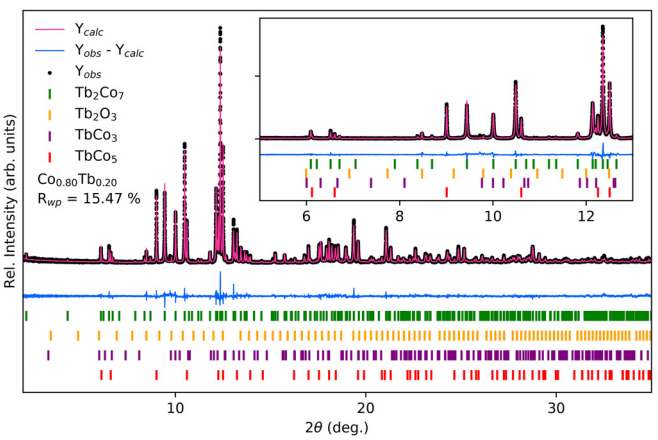

FIG. 1. High-resolution synchrotron powder XRD pattern of $Co_{0.80}Tb_{0.20}$ at room temperature (about 295 K), inset shows a zoomed-in figure of the low angle reflections. Tick marks representing the corresponding binary phases are shown below the calculated, observed, and difference curves from Rietveld analysis. Nominal composition and fit statistics are summarized in the figure.

TABLE I. Compositional and magnetic analysis of arc-melted Co–Tb alloys from Rietveld refinement of synchrotron powder XRD and powder magnetization measurements. The first five columns display the phase fraction of the Co–Tb and Tb–O phases present in the samples as extracted from Rietveld analysis of powder XRD data. Elemental analysis from EDS is compared to calculated elemental composition of the entire sample from phase fractions of each binary phase present. All errors shown in parentheses for corresponding quantities. The final two columns show the saturation magnetization (where applicable) taken from the maximum magnetization measured at 2 T applied external field and the necessary coercive field for sample at room temperature.

	% Co_2Tb	% Co_3Tb	% Co_7Tb_2	% Co_5Tb	% Tb_2O_3	EDS analysis	Calc. Comp.	$M_{sat.}$ (emu/g)	H_c (mT)
$Co_{0.66}Tb_{0.33}$	86.8(2)	7.25(9)	···	1.87(2)	4.05(2)	$Co_{0.67}Tb_{0.32}$	$Co_{0.664}Tb_{0.336}$	···	5.2
$Co_{0.70}Tb_{0.30}$	47.45(8)	40.21(9)	···	7.31(5)	5.02(4)	$Co_{0.48}Tb_{0.52}$	$Co_{0.696}Tb_{0.294}$	···	3.5
$Co_{0.72}Tb_{0.28}$	36.27(5)	53.23(7)	···	7.79(4)	2.69(2)	$Co_{0.72}Tb_{0.27}$	$Co_{0.725}Tb_{0.275}$	24	2
$Co_{0.74}Tb_{0.26}$	16.14(5)	66.1(1)	···	12.25(5)	5.54(3)	$Co_{0.74}Tb_{0.26}$	$Co_{0.735}Tb_{0.265}$	29	4
$Co_{0.76}Tb_{0.24}$	5.25(3)	89.1(1)	···	2.72(3)	2.86(3)	$Co_{0.75}Tb_{0.25}$	$Co_{0.740}Tb_{0.260}$	17.8	4.5
$Co_{0.78}Tb_{0.22}$	···	13.2(1)	82.1(7)	3.63(5)	1.00(2)	$Co_{0.77}Tb_{0.23}$	$Co_{0.776}Tb_{0.224}$	17.5	6
$Co_{0.80}Tb_{0.20}$	···	13.1(3)	61.1(1)	23.97(8)	0.77(1)	$Co_{0.79}Tb_{0.21}$	$Co_{0.785}Tb_{0.215}$	16	7
$Co_{0.82}Tb_{0.18}$	···	···	32.46(9)	66.0(1)	1.52(2)	$Co_{0.81}Tb_{0.19}$	$Co_{0.801}Tb_{0.193}$	19	5

sample, is in very close agreement with the targeted composition for each sample. The composition of $Co_{0.70}Tb_{0.30}$ from EDS has a large discrepancy from the nominal composition and XRD refinement. One explanation is possible Tb–O binaries in proximity to the measurements on the cleaved surface of this sample as EDS is a probe of local composition as compared to XRD as a probe of average composition. All samples show a very small phase fraction of Tb_2O_3 likely due to oxidation of the Tb starting material. Tb_2O_3 has a reported antiferromagentic transition at 2.42 K which is well below the temperature region for which this work is focused so its magnetic contribution is not discussed at length.[32] Supplementary material shows the evolution of the lattice parameters of each binary phase in the samples. For every binary phase, the lattice parameters show very little change between samples and thus it is clear any observable changes in magnetism amongst them is solely due to the relative phase fractions of the binaries present. The remaining paragraph of this Letter will address the composite magnetic properties of these samples corresponding to the different binaries present and how they interact to yield magnetic behavior similar to previous thin film work in the bulk.[23,27,28]

The magnetic properties of the Co-rich end of the Co–Tb phase diagram have been shown to be ideal for potential applications in SOT devices through thin film work.[23,26–29] We have done extensive crystallographic analysis for our samples to understand the Co–Tb alloys present in order to understand how the binaries combine to yield these

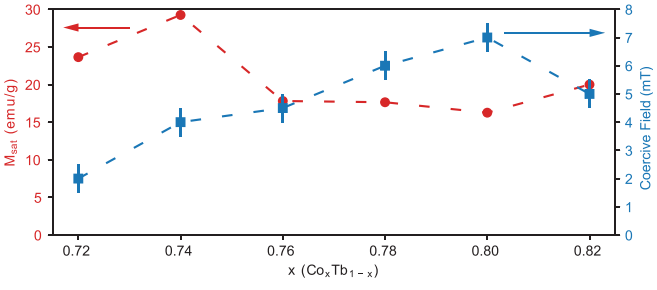

FIG. 2. Saturation magnetization taken from the maximum value in isothermal magnetization at room temperature measured up to 2 T applied external field and coercive field from the same measurement as a function of composition for Co_xTb_{1-x} (x = 0.72–0.82) samples.

desirable magnetic properties. The four Co–Tb binary alloys present in these samples are Co_2Tb, Co_3Tb, Co_7Tb_2, and Co_5Tb which have transition temperatures of 231 K, 509 K, 717 K, and 987 K, respectively.[33–38] In particular, the magnetic properties of Co_7Tb_2 have been reported less extensively than others. From these transition temperatures, it is clear that samples with Co_3Tb, Co_7Tb_2, and/or Co_5Tb are the most likely to house room temperature magnetic properties.

A summary of the most relevant magnetic measurement metrics at room temperature is given in Table I. As expected, the two compositions ($Co_{0.66}Tb_{0.32}$ and $Co_{0.70}Tb_{0.30}$) containing a majority phase of Co_2Tb display linear magnetization with respect to field as Co_2Tb is paramagnetic at room temperature. Both of these compositions show a clear ferrimagentic transition around 231 K which is well documented in the literature for the Co_2Tb compound and has been the focus of a large body of work.[33,39,40] However, due to these phases having no magnetic order around room temperature, they are not of particular interest for device applications and the magnetic data for these two compositions are shown in detail in supplementary material.

The magnetic property data on all compounds with $x > 0.70$ is shown in Fig. 3 and Table I displaying the temperature dependence of magnetization and field dependence of magnetization at room temperature. As the Co ratio is increased, the majority phases begin to become phases with room temperature magnetic order. For $Co_{0.72}Tb_{0.28}$, $Co_{0.74}Tb_{0.26}$, and $Co_{0.76}Tb_{0.24}$, the majority phase is Co_3Tb which orders ferrimagnetically at a temperature of 509 K which is well above room temperature.[34,41] The data shown in Fig. 3 reflects this showing all three compounds display predominate ferrimagnetic ordering at room temperature. All three of these compositions have some remaining Co_2Tb from Rietveld analysis which is supported by the additional magnetic transition around the 231 K range. For compositions $x > 0.76$, the majority phase becomes Co_3Tb, Co_7Tb_2, or Co_5Tb which all have transition temperature above 400 K and as such, their corresponding magnetic transitions are not observed in the data. The only transition we observe for highest Tb concentrations is the magnetic compensation point in Co_5Tb for the $Co_{0.82}Tb_{0.18}$ sample which has Co_5Tb as a phase majority.[42] For x = 0.72–0.76, we do observe that as the phase fraction of Co_3Tb increases, so does the magnetization at room temperature as the amount of Co_5Tb in each phase is negligible and the Co_2Tb is non-

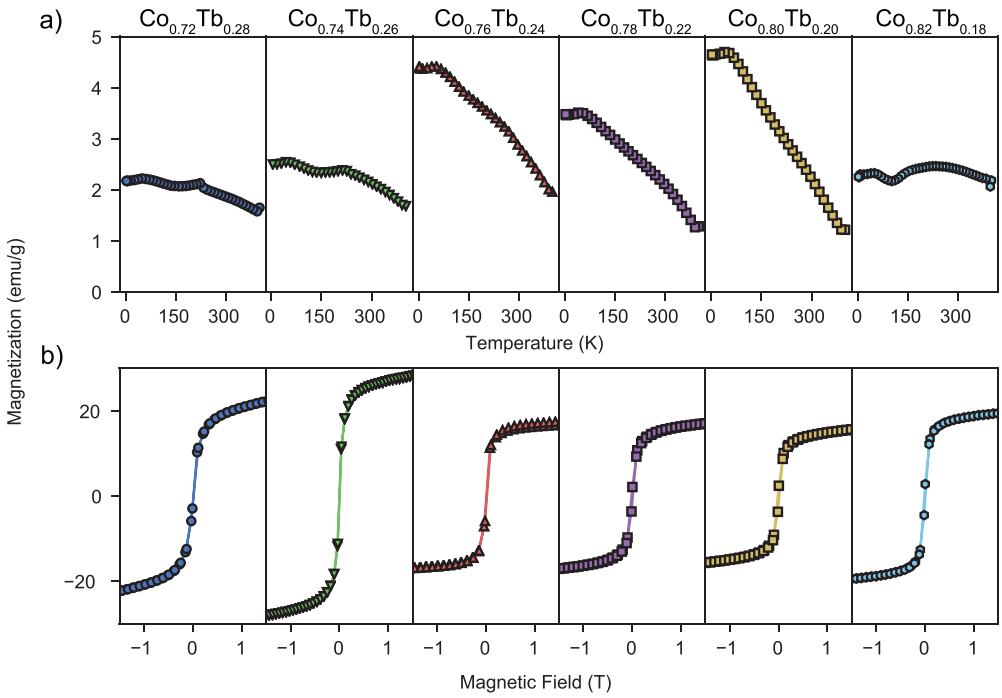

FIG. 3. (a) Temperature dependence of magnetization for Co_xTb_{1-x} ($x = 0.70 - 0.82$) measured from 400 K to 1.8 K with an applied field of H = 100 Oe and at ambient pressure. (b) Field dependence of magnetization of the same compositions measured from ±2 T at room temperature (300 K).

magnetic at room temperature. Table I shows the coercive field on all three compounds is low indicating the *f–d* magnetic coupling between antiparallel ordering of Co and Tb atoms is weak.[43,44]

Table I shows the last three compositions, $Co_{0.78}Tb_{0.22}$, $Co_{0.80}Tb_{0.20}$, and $Co_{0.82}Tb_{0.18}$, which have the most optimal magnetic properties at room temperature with regard to device usage. In this range, the magnetic saturation reaches a minimum while the coercive field reaches a maximum. From Rietveld analysis, $Co_{0.78}Tb_{0.22}$ and $Co_{0.80}Tb_{0.20}$ contain a majority Co_7Tb_2 while $Co_{0.82}Tb_{0.18}$ contains a majority of Co_5Tb. Both Co_7Tb_2 and Co_5Tb have magnetic transitions above room temperature, 717 and 987 K, respectively.[36–38] Figure 3 shows that once Co_5Tb becomes the majority phase ($Co_{0.82}Tb_{0.18}$ sample), the magnetization around room temperature and above is significantly higher than those with Co_7Tb_2 as the majority phase ($Co_{0.78}Tb_{0.22}$ and $Co_{0.80}Tb_{0.20}$). This is due to Co_7Tb_2 exhibiting a magnetic compensation point around 410 K where the magnetization reaches a minimum with respect to temperature and increases below this point.[35] The magnetic saturation of $Co_{0.78}Tb_{0.22}$ and $Co_{0.80}Tb_{0.20}$ in the field range up to 2 T is the lowest of all Co–Tb alloys, and this is paired with these two compositions exhibiting the largest coercive field. These properties can be justified by the Co_7Tb_2 phase having been shown to have the highest exchange field between Co and Tb atoms of the nearby phases using the high field free powder (HFFP) method.[44] Thus, $Co_{0.78}Tb_{0.22}$ and $Co_{0.80}Tb_{0.20}$ occupy the ideal composition range for device related properties in Table I and these results are in very close agreement with related thin film work on these compounds.[23,27,28]

From this bulk analysis, it would appear that the most important phase for desirable room temperature magnetic properties is the Co_7Tb_2 phase. To date, little work has been done on this phase specifically;[35,36,45] however, the phase is very closely related to the Co_5Tb phase and the two phases have been reported to form as a mixture which is supported by our Rietveld analysis.[35] Single crystals of Tb_2Co_7 have been reported so a full analysis of the magnetic properties of this phase could be pursued especially when integrating single crystals into possible device stacks. Additionally, the magnetic compensation point at 410 K for Co_7Tb_2 could be very beneficial for application and this high temperature region must be explored more closely.

We have performed high pressure magnetometry measurements of polycrystalline ingots of these Co–Tb alloys to understand its effects on the magnetic properties of this system. Compositions that contain significant amounts of Co_2Tb ($x = 0.66–0.74$) where the ferrimagnetic transition around 230 K is observable in magnetization with respect to temperature show the most discernible change with external pressure. These changes are shown in supplementary material for each composition and match previous reports of how external pressure changes the ferrimagentic transition in Co_2Tb by decreasing the transition temperature with increasing pressure.[46,47] The remaining Co–Tb binaries all have transition temperatures above the measured range and as such do not change as drastically. However, we are focused on showing how the magnetic properties of these phases change around room temperature. In summary, for all the remaining compositions, the only noticeable pressure-induced changes in magnetic properties are small changes in magnetization saturation with respect to field and

magnetization magnitude at different temperatures which are shown in supplementary material for all $Co_{1-x}Tb_x$ compositions. From these we see that magnetic saturation scales linearly for all samples across the range of applied pressure and for all temperatures at which isothermal magnetization was measured.

Most importantly, Fig. 4 shows how the magnetic properties of the composition $Co_{0.80}Tb_{0.20}$ change at various external pressure. As expected, magnetization with respect to temperature shows very little change with pressure with slightly higher magnetization at high pressures. Interestingly, this increase in magnetization does become smaller at higher temperatures as the temperature approaches the magnetic compensation point in Co_7Tb_2, which is the majority phase in this composition.[35] Field dependence of magnetization shows the magnetic saturation in $Co_{0.80}Tb_{0.20}$ does increase with added pressure by around 10% at 2 T applied field. However, the coercive field at room temperature shows virtually no change with added pressure. This work shows that the magnetic properties of higher Co-ratio Co–Tb alloys present in these systems (Co_3Tb, Co_7Tb_2, and Co_5Tb) have little pressure dependence below 400 K. This is likely due to the high ferrimagnetic transition temperatures of these compounds.[34–38] Future work could explore negative pressure applied through strain on these compositions as well as chemical pressure through doping to tune the magnetic properties around room temperature.

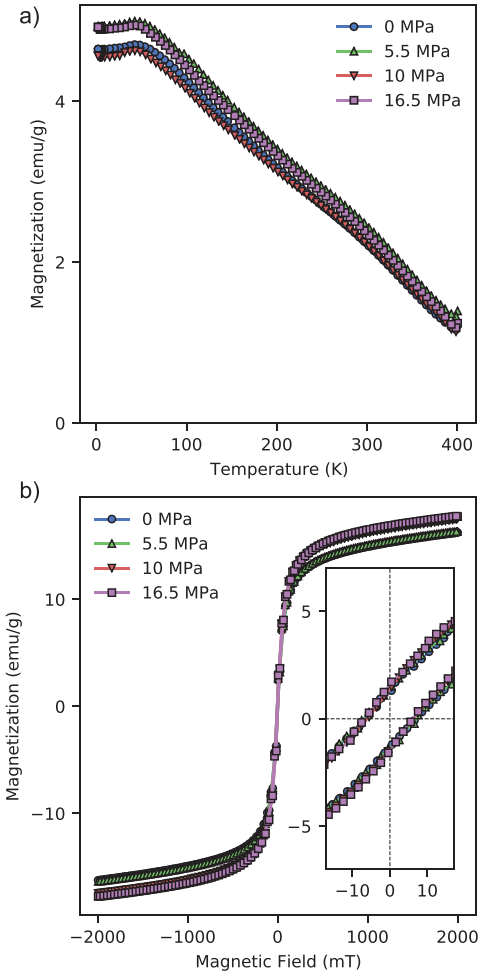

FIG. 4. (a) Temperature-dependent magnetization of $Co_{0.80}Tb_{0.20}$ at various applied pressures with an applied field of 100 Oe and (b) field-dependent magnetization of $Co_{0.80}Tb_{0.20}$ at various applied pressures at 300 K. The inset shows the low field range of field-dependent magnetization to emphasize the coercive field change with respect to external pressure.

In summary, we have synthesized a full range of multiphase Co–Tb alloys across the composition range Co_xTb_{1-x} (x = 0.66–0.82) in order to study the bulk properties of the compounds in this region. Through systematic compositional analysis of high-resolution powder XRD and elemental analysis, we have shown the phases present and phase fraction of these phases in each compound. The phases present and their relative phase fractions follow the known phase diagram and give a foundation to analyze the magnetic properties of these compounds on the basis of the composition. As such, we have completed a full analysis of the magnetic properties of these compounds and show that these compounds behave in line with the binaries present as well as previous thin film work. With respect to previous thin film work which showed optimal magnetic properties for SOT devices in the region of $x = 0.78$, we have seen similar results in bulk samples in this composition range. Importantly, $Co_{0.78}Tb_{0.22}$ and $Co_{0.80}Tb_{0.20}$ show a minimum in magnetic saturation at 2 T and maximum in coercive field at room temperature. We attribute these properties to the majority phase in each compound, Co_7Tb_2, which is the least studied Co–Tb binary present in this phase space.[35,36,45] We have then explored the effects of high pressure on the magnetic order and behavior in these compositions in the temperature range below 400 K. Our work shows that high pressure only significantly changes the magnetism in compounds containing Co_2Tb in this temperature range.[33–38] This work bridges the gap between recent thin film work, which shows Co–Tb alloys display ideal properties for SOT devices, and bulk synthesis to understand which phases give rise to these properties and can be targeted for future exploration. Of these binary phases, Co_7Tb_2 is the least studied and majority phase in the optimal composition range of these compounds. Thus, future work on thin film or single crystal synthesis and magnetic/transport properties of Co_7Tb_2 would be needed to understand the properties of this binary and how it can be best used for spintronic devices.

See the supplementary material for the additional data. Additional data contains high-resolution XRD data for all Co_xTb_{1-x} samples with accompanying Rietveld refinements with data summarized in Table I of the main text. Magnetometry data for all Co_xTb_{1-x} samples is included as well, with temperature-dependent magnetization at different pressures, field-dependent magnetization at 300 K and various pressures, and field-dependent magnetization at various pressure at ambient pressure.

Research at the United States Naval Academy was supported by the NSF DMR-EPM 1904446 and ONR 1400844839. Use of the Advanced Photon Source at Argonne National Laboratory was supported by the U.S. Department of Energy, Office of Science, Office of Basic Energy Sciences, under Contract No. DE-AC02-06CH11357. This work was supported by the U.S. Office of Naval Research through the Naval Research Laboratory's basic research

program. D.A. Gilbert and W.L.N.C.L. acknowledge support by the U.S. Department of Energy, Office of Basic Research under Award No. DE-SC0021344.

DATA AVAILABILITY

The data that support the findings of this study are available from the corresponding author upon reasonable request.

REFERENCES

[1]L. Berger, Phys. Rev. B **54**, 9353 (1996).
[2]J. Slonczewski, J. Magn. Magn. Mater. **159**, L1 (1996).
[3]I. Žutić, J. Fabian, and S. D. Sarma, Rev. Mod. Phys. **76**, 323 (2004).
[4]A. Hoffmann and S. D. Bader, Phys. Rev. Appl. **4**, 047001 (2015).
[5]T. Jungwirth, X. Marti, P. Wadley, and J. Wunderlich, Nat. Nanotechnol. **11**, 231 (2016).
[6]C. Chappert, A. Fert, and F. N. Van Dau, in *Nanoscience and Technology: A Collection of Reviews from Nature Journals* (World Scientific, 2010), pp. 147–157.
[7]E. Myers, D. Ralph, J. Katine, R. Louie, and R. Buhrman, Science **285**, 867 (1999).
[8]F. J. Jedema, A. Filip, and B. Van Wees, Nature **410**, 345 (2001).
[9]Y. Huai, F. Albert, P. Nguyen, M. Pakala, and T. Valet, Appl. Phys. Lett. **84**, 3118 (2004).
[10]D. Worledge, G. Hu, D. W. Abraham, J. Sun, P. Trouilloud, J. Nowak, S. Brown, M. Gaidis, E. O'sullivan, and R. Robertazzi, Appl. Phys. Lett. **98**, 022501 (2011).
[11]A. Manchon and S. Zhang, Phys. Rev. B **79**, 094422 (2009).
[12]R. Ramaswamy, J. M. Lee, K. Cai, and H. Yang, Appl. Phys. Rev. **5**, 031107 (2018).
[13]Y. Li, K. W. Edmonds, X. Liu, H. Zheng, and K. Wang, Adv. Quantum Technol. **2**, 1800052 (2019).
[14]V. Baltz, A. Manchon, M. Tsoi, T. Moriyama, T. Ono, and Y. Tserkovnyak, Rev. Mod. Phys. **90**, 015005 (2018).
[15]J. Železný, P. Wadley, K. Olejník, A. Hoffmann, and H. Ohno, Nat. Phys. **14**, 220 (2018).
[16]Y. Xu, S. Wang, and K. Xia, Phys. Rev. Lett. **100**, 226602 (2008).
[17]P. Merodio, A. Kalitsov, H. Béa, V. Baltz, and M. Chshiev, Appl. Phys. Lett. **105**, 122403 (2014).
[18]R. Cheng, M. W. Daniels, J.-G. Zhu, and D. Xiao, Phys. Rev. B **91**, 064423 (2015).
[19]X. Chen, X. Zhou, R. Cheng, C. Song, J. Zhang, Y. Wu, Y. Ba, H. Li, Y. Sun, Y. You, Y. Zhao, and F. Pen, Nat. Mater. **18**, 931 (2019).
[20]T. I. Fitchorov, S. Bennett, L. Jiang, G. Zhang, Z. Zhao, Y. Chen, and V. G. Harris, Acta Mater. **73**, 19 (2014).
[21]P. Hansen, C. Clausen, G. Much, M. Rosenkranz, and K. Witter, J. Appl. Phys. **66**, 756 (1989).
[22]K. Buschow, J. Appl. Phys. **51**, 2795 (1980).
[23]J. Finley and L. Liu, Phys. Rev. Appl. **6**, 054001 (2016).
[24]N. Roschewsky, T. Matsumura, S. Cheema, F. Hellman, T. Kato, S. Iwata, and S. Salahuddin, Appl. Phys. Lett. **109**, 112403 (2016).
[25]Z. Zheng, Y. Zhang, X. Feng, K. Zhang, J. Nan, Z. Zhang, G. Wang, J. Wang, N. Lei, D. Liu, Y. Zhang, and W. Zhao, Phys. Rev. Appl. **12**, 044032 (2019).
[26]H. Wang, J. Finley, P. Zhang, J. Han, J. T. Hou, and L. Liu, Phys. Rev. Appl. **11**, 044070 (2019).
[27]S. A. Siddiqui, J. Han, J. T. Finley, C. A. Ross, and L. Liu, Phys. Rev. Lett. **121**, 057701 (2018).
[28]T. H. Pham, S.-G. Je, P. Vallobra, T. Fache, D. Lacour, G. Malinowski, M. C. Cyrille, G. Gaudin, O. Boulle, M. Hehn, J.-C. Rojas-Sánchez, and S. Mangin, Phys. Rev. Appl. **9**, 064032 (2018).
[29]S.-G. Je, J.-C. Rojas-ánchez, T. H. Pham, P. Vallobra, G. Malinowski, D. Lacour, T. Fache, M.-C. Cyrille, D.-Y. Kim, S.-B. Choe, M. Belmeguenai, M. Hehn, S. Mangin, G. Gaudin, and O. Boulle, Appl. Phys. Lett. **112**, 062401 (2018).
[30]B. H. Toby and R. B. Von Dreele, J. Appl. Crystallogr. **46**, 544 (2013).
[31]H. Okamoto and H. Okamoto, *Phase Diagrams for Binary Alloys* (ASM international Materials Park, OH, 2000), Vol. 314.
[32]R. Hill, J. Phys. C **19**, 673 (1986).
[33]M. Halder, S. Yusuf, M. Mukadam, and K. Shashikala, Phys. Rev. B **81**, 174402 (2010).
[34]R. Tetean, E. Burzo, and I. Deac, J. Alloys Compd. **442**, 206 (2007).
[35]R. Lemaire, "Magnetic properties of the intermetallic compounds of cobalt with the rare earth metals and yttrium," Cobalt **33**, 201–211 (1966).
[36]H. Yoshie, T. Kojima, M. Hoshino, Y. Amako, H. Nagai, K. Adachi, M. Shiga, and Y. Nakamura, J. Phys. Soc. Jpn. **64**, 2241 (1995).
[37]Z. Tie-Song, J. Han-Min, G. Guang-Hua, H. Xiu-Feng, and C. Hong, Phys. Rev. B **43**, 8593 (1991).
[38]T. Okamoto, H. Fujii, C. Inoue, and E. Tatsumoto, J. Phys. Soc. Jpn. **34**, 835 (1973).
[39]K. Zhou, Y. Zhuang, J. Li, J. Deng, and Q. Zhu, Solid State Commun. **137**, 275 (2006).
[40]D. Gignoux, F. Givord, R. P. de la Bathie, and F. Sayetat, J. Phys. F **9**, 763 (1979).
[41]R. Tetean and E. Burzo, J. Magn. Magn. Mater. **272–276**, E599 (2004).
[42]R. Ballou, B. Gorges, R. Lemaire, H. Rakoto, and J. Ousset, Phys. B: Condens. Matter **155**, 266 (1989).
[43]S. Kervan and N. Kervan, J. Supercond. Novel Magn. **24**, 819 (2011).
[44]J. Liu, F. De Boer, P. De Châtel, R. Coehoorn, and K. Buschow, J. Magn. Magn. Mater. **132**, 159 (1994).
[45]A. Andreev, E. Tarasov, A. Deryagin, and S. Zadvorkin, Phys. Status Solidi A **71**, K245 (1982).
[46]E. Burzo, P. Vlaic, D. Kozlenko, S. Kichanov, N. Dang, E. Lukin, and B. Savenko, J. Alloys Compd. **551**, 702 (2013).
[47]B. Ahuja, H. Mund, J. Sahariya, A. Dashora, M. Halder, S. Yusuf, M. Itou, and Y. Sakurai, J. Alloys Compd. **633**, 430 (2015).